Direct numerical simulations of oscillatory wall-bounded flow over a closely-packed fixed bed of spherical particles

By C. Ghodke†, S. Apte† AND J. Urzay

A number of hurdles remain in the development of predictive models for sediment transport. One of these, for instance, is the characterization of particular flow conditions leading to incipient motion. In order to study transport of sediments, a detailed knowledge of the oscillatory flow over the near-bed sediment layer is required. In this study, direct numerical simulations (DNS) are performed using a fictitious domain approach (Apte & Finn 2013) to investigate the effect of an oscillatory flow field over a rough wall made up of a regular hexagonal pack of fixed spherical particles, in a setup similar to the experimental configuration of Keiller & Sleath (1976). Transitional and turbulent flows at Reynolds numbers $\mathrm{Re}_\delta = 95, 150, 200, 400$ and 685 (based on the Stokes-layer thickness δ) are studied. Characterizations of the resulting flow fields are performed in terms of coherent vortex structures, turbulent kinetic-energy budgets, cross-correlations between forces upon particles and flow variables, along with statistical distributions of near-bed velocities and pressure fluctuations. The unsteady hydrodynamic lift forces on particles and their cross-correlations with sweep and burst events are also studied. Results show that the lift coefficient is maximized when the strength of the sweep and ejection events is maximum. In addition, its value is well correlated with phase-averaged near-bed velocity, although the cross-correlation decays rapidly away from the particle. On the other hand, the lift-force fluctuations become positively and negatively correlated with pressure in the front and aft neighborhood of the the particle due to wake effects. Statistical analyses show that the near-bed velocity and pressure fluctuations fit poorly with Gaussian distribution. Instead, a fourth order Gram-Charlier distribution model is proposed that may have consequences on the Gaussian descriptions of sediment pick-up functions typically used in quantifications of turbulent transport of sediments.

1. Introduction

Sediment particles in close contact with each other are often found in river and sea beds (Fredsøe & Deigaard 1992). Shear stresses above a threshold brought by fluid flow can mobilize and transport these particles from the bed. The prediction of erosion onset, also known as incipient motion, and its interdependence on oscillatory turbulent shear stresses, are two long-standing issues governing sediment transport in coastal environments. Computations of sediment-laden flows typically employ simplistic models (Fredsøe & Deigaard 1992; Nelson *et al.* 2000), including Shield's or Sleath's parameter models (Sleath 1995; Flores & Sleath 1998), which are based on a critical or threshold value of bed shear stress or peak pressure gradient, beyond which particle motion takes place. However, these models are deterministically based on mean values of the bed shear stresses, and do not consider particle size, shape, bed arrangements, or multi-scale interactions

† School of Mechanical, Industrial and Manufacturing Engineering, Oregon State University

Re_δ	Re_D	k_s^+	Nx	Ny	Nz	Nz/D	$\Delta x^+, \Delta y^+, \Delta z^+_{min}, \Delta z^+_{max}$	Total
95	660	90	136	80	460	160	2.3, 2.2, 0.5, 1.1	5M
150	1042	140	124	100	556	200	4, 2.8, 0.7, 1.5	7M
200	1390	190	208	120	664	240	3.1, 3.1, 0.8, 1.7	17M

TABLE 1. Computational parameters and grid resolution details

between oscillatory turbulent flow and sediment particles. On the other hand, stochastic models of incipient motion, based on modeling the probability of particle entrainment, hold promise in accounting for the intermittent dynamics of turbulent flows. Additionally, in many instances, computations or measurements of drag and lift forces are not straightforward. Instead, they are calculated indirectly by assuming a cross-correlation with Gaussian or log-normal near-bed velocity fluctuations (Einstein 1950; Papanicolaou *et al.* 2002; Cheng & Law 2003; Wu & Chou 2003; Wu & Kuo-Hsin 2004; Hofland & Battjes 2006). It is unclear, however, whether the cross-correlation persists over the entire oscillation cycle and to what extent is dependent on the sampling spatial location.

As a first step towards a fundamental understanding of sediment incipient motion in coastal environments, a DNS of an oscillatory boundary layer over a closely packed sediment particles is performed here, with the sediment particles being held fixed to the substrate. The unsteady forces on the particles and their correlations with the oscillatory turbulent flow characteristics are quantified, along with the statistical distribution of the near-bed velocity and pressure fluctuations. The remainder of this report is structured as follows. The computational setup is outlined in Section 2. In Section 3 simulation results, including force and turbulence statistics are presented. Finally, conclusions are drawn in Section 4.

2. Methodology

The computational domain, which is shown in Figure 1, consists of a doubly periodic box (in x and y directions) with a smooth non-slip wall at $z = 0$ and a slip wall at $z = 30\delta$, where $\delta = \sqrt{2\nu/\omega}$ is the Stokes-layer thickness. In this formulation, ν is the kinematic viscosity, and ω is the oscillation frequency. The in-plane domain length is 24.1δ and 13.9δ in the streamwise and spanwise directions, respectively. The particle diameter normalized with the Stokes-layer thickness, $D = d/\delta = 6.95$, affords only 13 particles in the domain. Although a similar computational setup was used in previous work from other group (Fornarelli & Vittori 2009), clear limitations arise in the use of DNS, in that larger domain sizes are most likely required in the presence of such large particles for results to approach statistically significant dynamics, a subject which is presently under investigation.

The dimensionless parameters of the problem, which are outlined in Table 1, consist of the particle Reynolds number $\mathrm{Re}_D = U_\infty D/\nu$, the Reynolds number based on Stokes-layer thickness $\mathrm{Re}_\delta = U_\infty \delta/\nu$, and the effective roughness Reynolds number $k_s^+ = u_\tau D/\nu$, the latter being in the fully rough regime (Jensen *et al.* 1989). In this formulation, U_∞ is the amplitude of the free-stream velocity profile, and u_τ is the friction velocity. A systematic grid resolution study was performed for various Reynolds numbers to obtain optimum grid spacing as given in Table 1. A hyperbolic tangent function was used to stretch the mesh in the wall normal direction. The numerical algorithm, developed by

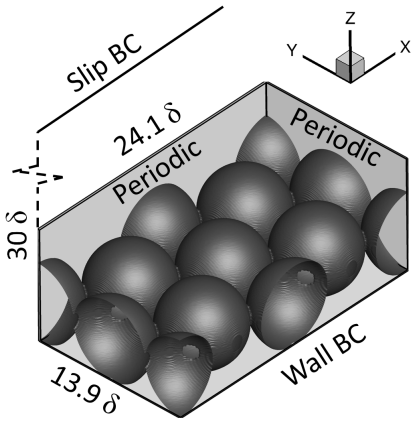

FIGURE 1. Schematic of the computational domain and boundary conditions. A sinusoidal pressure forcing is imposed that results in a streamwise velocity component $U_\infty \sin(\omega t)$ far from the bed.

Apte & Finn (2013) is used in the present work. The computational setup was verified and validated at $\mathrm{Re}_\delta = 95$ by using experiments of Keiller & Sleath (1976) and earlier computations made by Fornarelli & Vittori (2009) and (Ding & Zhang 2010). Details of the validation study can be found elsewhere (Ghodke *et al.* 2014).

3. Numerical results

For illustration purposes, results of the force and turbulent field analysis are presented only for $\mathrm{Re}_\delta = 150$ and 200, with 20 flow cycles run per case. The discussion of the results begins with a brief characterization of turbulent structures over a single cycle, followed by turbulent-kinetic energy budgets and spatio-temporal statistics.

The flow structures present in the near-bed region interact with the particles and generate instantaneous forces that can lead to incipient motion. Instantaneous near-bed flow structures are identified in Figure 2 in the form of λ_2-isosurfaces as described in earlier vorticity-identification studies (Jeong & Hussain 2006). While the effective Reynolds number Re_δ near the zero-velocity phase is much smaller than the one listed in Table 1, decaying turbulent fluctuations remain as a result of the imposed flow acceleration. As the velocity increases, the flow undergoes transition to fully turbulent dynamics, with a complex forest of low-speed streaks, whose density increases with increasing Re_δ, becoming elongated in the streamwise direction and reaching a maximum activity near the point of maximum velocity in the oscillation cycle. The presence of these structures was speculated by Keiller & Sleath (1976), although the experimental technique utilized there impeded their correct visualization. A fundamental question then arises as to what extent these near-wall structures influence the instantaneous forces on the particles and how can their effect be incorporated in stochastic models of incipient motion.

Turbulent kinetic-energy (TKE) budget terms are plotted over half a cycle at various distances from the wall ($z/D = 1.01$ and $z/D = 1.15$) for $\mathrm{Re}_\delta = 150$ and 200 in Figures 3 and 4, respectively. Specifically, the plots report TKE variations due to production, dissipation, turbulent transport, pressure transport, and viscous diffusion. Of particular interest is to notice the turbulent production-dissipation dominance at sufficiently long distances from the wall, $z/D = 1.15$, although both quantities are never in balance

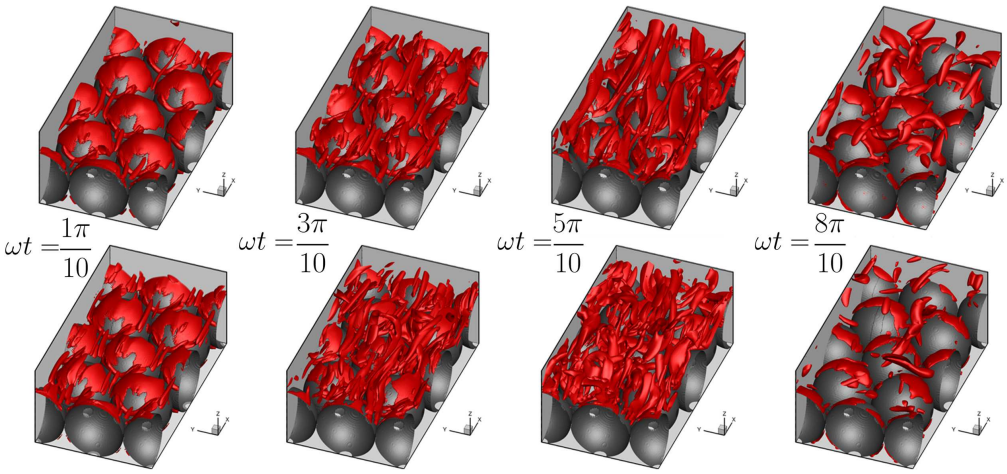

FIGURE 2. Instantaneous isosurfaces of the λ_2-parameter (Jeong & Hussain 2006) for different phases in the flow cycle, for $\mathrm{Re}_\delta = 150$ (top row), and $= \mathrm{Re}_\delta = 200$ (bottom row). The flow direction is from lower left to upper right.

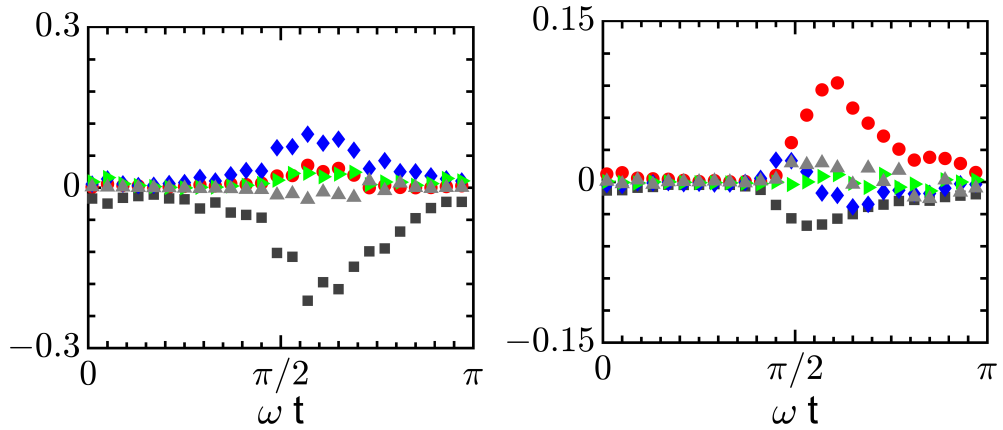

(a) $z/D = 1.015$ (b) $z/D = 1.15$

FIGURE 3. Phase-averaged TKE budget for $\mathrm{Re}_\delta = 150$. Symbols represent: ●, production; ■, dissipation; ♦, viscous diffusion; ►, pressure transport; ▲, turbulent transport.

because of the statistical non-stationarity induced by the flow acceleration, which leads to time variations of TKE during the flow cycle. Similarly, as the Reynolds number increases, the peaks in the production and dissipation, are observed much earlier in the flow cycle, indicating a prompt transition to fully turbulent regimes. Such turbulent states are strongly influenced by sweeps and ejections, as shown in the quadrant analysis (Kim *et al.* 2006) in Figure 5, whereas the contribution from inward and outward motions to the Reynolds stresses is marginal.

Figure 6 plots the variation of both phase-averaged lift coefficient and the square of the normalized streamwise velocity above the sediment bed for $\mathrm{Re}_\delta = 200$. The net lift coefficient has a period of half the forcing function plus a short phase delay. The phase-averaged lift force is found to be well correlated with the corresponding phase-averaged squared velocity above the sediment bed, albeit the small phase difference.

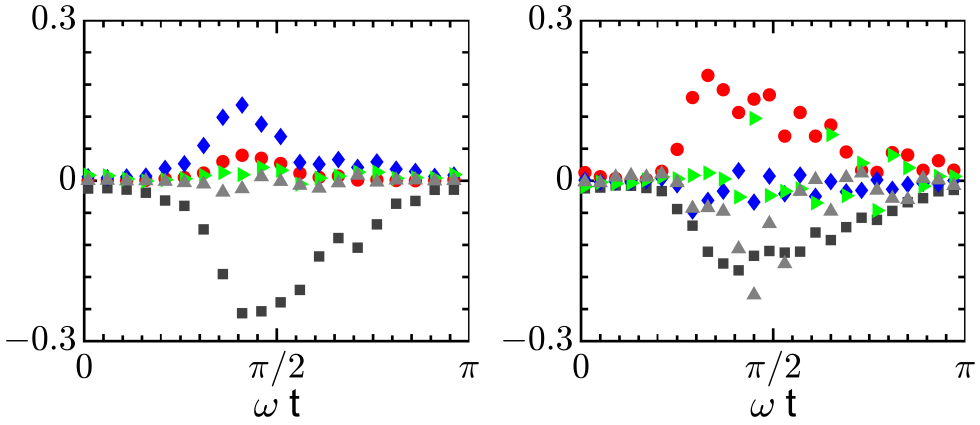

(a) $z/D = 1.015$ (b) $z/D = 1.15$

FIGURE 4. Phase-averaged TKE budget for $\mathrm{Re}_\delta = 200$. Symbols represent: ●, production; ■, dissipation; ♦, viscous diffusion; ►, pressure transport; ▲, turbulent transport.

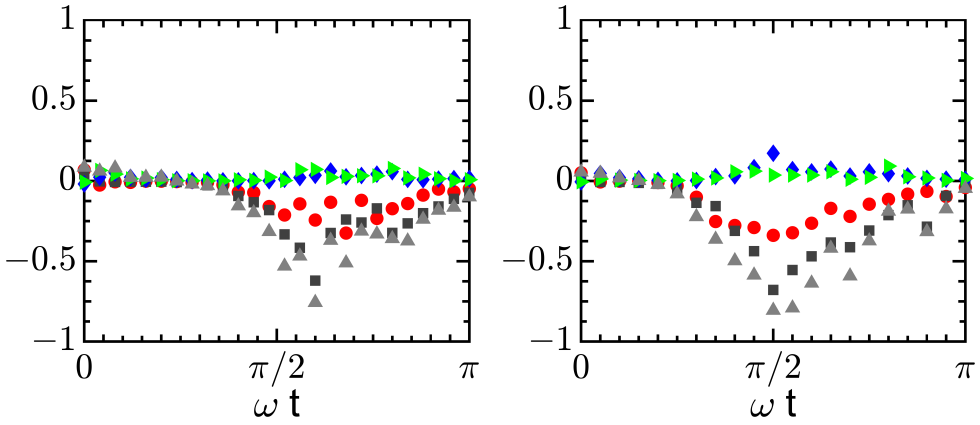

(a) $\mathrm{Re}_\delta = 150$ (b) $\mathrm{Re}_\delta = 200$

FIGURE 5. Phase variation of the contribution towards the Reynolds stress from ejection, sweep, inward and outward motions plotted above the crest of the sphere at $z/D = 1.15$ for $\mathrm{Re}_\delta = 150$ and 200. Symbols represent: ●, sweep; ■, ejection; ♦, inward; ►, outward; ▲, Reynolds stress.

Based on these results, two questions arise as to what is the distribution of the near-bed velocity and to what spatial extent it is cross-correlated with the lift force. To answer the former, Figure 7(a) shows the probability-density function (PDF) of the near-bed velocity fluctuations in the region above the particle for $\mathrm{Re}_\delta = 200$, and at the phase at which the Reynolds stress is maximum. Rather than Gaussian, the resulting PDF fits well with the fourth-order Gram-Charlier model (Wu & Kuo-Hsin 2004)

$$f_{GC4}(\phi') = \frac{\exp(-\phi'^2/2)}{\sqrt{2\pi}}\left[1 + \frac{S_\phi}{3!}(\phi'^3 - 3\phi') + \frac{F_\phi - 3}{4!}(\phi'^4 - 6\phi'^2 + 3)\right], \qquad (3.1)$$

where ϕ' is the normalized fluctuating flow variable, S_ϕ and F_ϕ are skewness and flatness of its distribution, respectively.

To evaluate the spatial extent of the cross-correlation between the lift force and the streamwise velocity fluctuations, the phase-averaged three-dimensional correlation func-

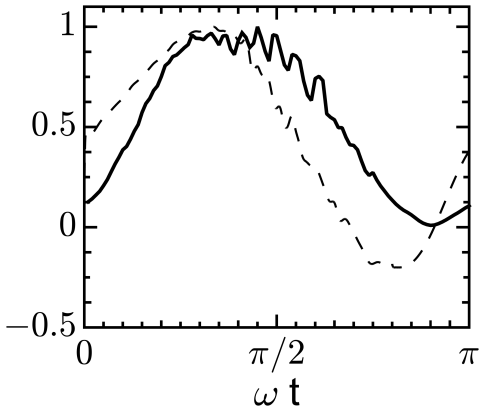

FIGURE 6. Phase-averaged time variation of the lift coefficient (dashed line) and normalized near-bed streamwise velocity squared (solid line) for $\mathrm{Re}_\delta = 200$.

tion

$$R_{F',\phi'}(\Delta x, \Delta y, z, t) = \frac{1}{N_t N_p} \sum_{i=1}^{N_t} \sum_{j=1}^{N_p} \phi' \left[(x_{p,j} + \Delta x), (y_{p,j} + \Delta y), z, t_i)\right] F'(x_{p,j}, y_{p,j}, z_{p,j}, t_i) \qquad (3.2)$$

is computed in a similar manner as done by Chan-Braun *et al.* (2013) for a non-oscillatory flow over a bed of smaller particles, where F' is the particle force fluctuations, ϕ' is the flow variable fluctuations, the sub-index $_p$ refers to the particle position, and N_p and N_t are the number of particles and number of per-phase time snapshots, respectively. Figure 8 presents contours of spatial cross-correlations of velocity and pressure fluctuations with the fluctuating lift force on the particles, indicating the region of influence of the near-bed turbulence on the particle hydrodynamic force. As shown in Figure 8(a), the lift force is found to be positively correlated with velocity fluctuations in the region above the particle crest, more positively so at around one diameter distance downstream from the particle. A more intricate behavior is noted in Figure 8(b) for the pressure perturbations, which, in addition to being strongly non-Gaussian (e.g. see Figure 7(b)), are correlated and anti-correlated with the lift force in the front and aft regions of the particle, respectively; this effect being related to the strong wakes induced by the relatively high particle Reynolds numbers.

4. Conclusions

DNS of transitional and turbulent oscillatory flows over a fixed layer of hexagonally packed sediment particles corresponding to the experimental setup of Keiller & Sleath (1976) were performed. The flow over the particles was characterized in terms of coherent vortex structures, TKE budgets, PDF distributions for velocity and pressure perturbations, and their cross-correlations with the lift force. The turbulent flow structures were analyzed in detail to show the presence of a complex forest of low-speed streaks as a consequence of ejection and sweep motions. The lift coefficient reached maximum value simultaneously with the maximum intensity of the sweep and ejection motions. The phase-averaged lift force has a period of half the forcing function and was found to be well correlated with the phase-averaged velocity fluctuations above the bed, with a small

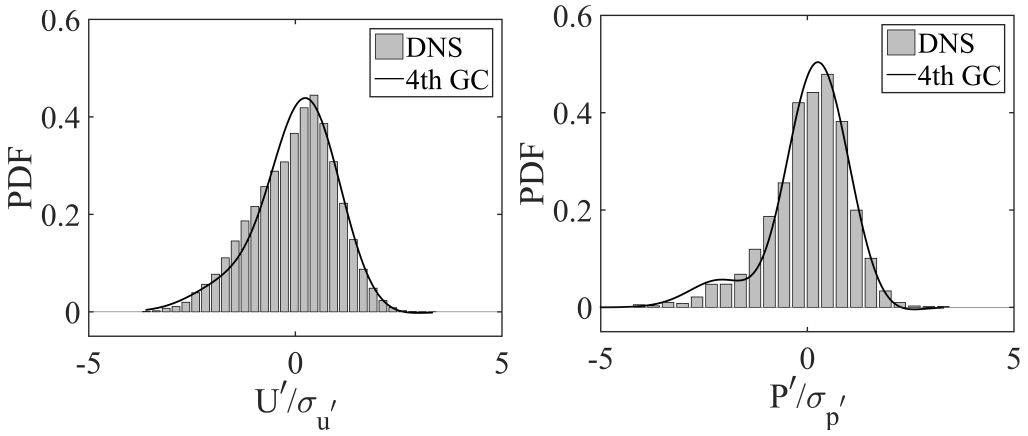

(a) PDF of velocity fluctuations (u') (b) PDF of pressure fluctuations (p')

FIGURE 7. PDF of normalized streamwise velocity and pressure fluctuations for $\mathrm{Re}_\delta = 200$ at the peak phase $\omega t = \pi/2$. DNS data is represented by histograms and solid line represents fourth-order Gram-Charlier distribution. Data is taken in the two stokes layer thickness above the crest of the particle. Horizontal axes are normalized with standard deviations.

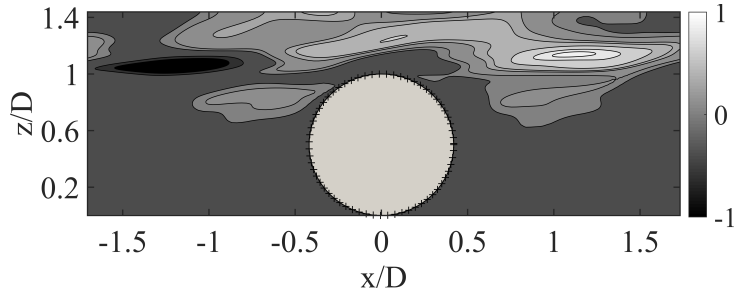

(a) lift force and velocity correlation

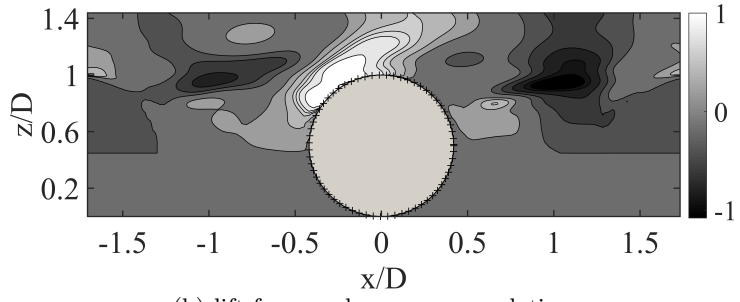

(b) lift force and pressure correlation

FIGURE 8. Spatio-temporal correlation function of lift force and velocity and pressure fluctuations for $\mathrm{Re}_\delta = 200$. Correlation function field is plotted for the phase at which lift coefficient is maximum. Particle periphery is denoted by symbol +.

phase difference. The PDF distributions of the velocity and pressure fluctuations showed a non-Gaussian behavior that followed a fourth-order Gram-Charlier distribution. The three-dimensional correlation function revealed that the lift force is well correlated with the streamwise velocity fluctuations up to distances of the same order as the particle

diameter, beyond which the cross correlation decays considerably. On the other hand, the pressure fluctuations were correlated and anti-correlated with the lift force in the front and aft regions of the particle respectively, as a result of wake flows.

Acknowledgments

The first two authors acknowledge the National Science Foundation (NSF) for the award NSF-CBET project number 1133363. The computations were performed on the Texas Advanced Computing Center, Lonestar machine. In addition, they would also like to thank Prof. Ali Mani for providing local computer resources during the Summer Program, and Jeremy Horwitz for reviewing this report.

REFERENCES

Apte, S. V. & Finn, J. R. 2013 A variable-density fictitious domain method for particulate flows with broad range of particle-fluid density ratios. *J. Comput. Phys.* **243**, 109–129.

Chan-Braun, C., Garcia-Villalba, M. & Uhlmann, M. 2013 Spatial and temporal scales of force and torque acting on wall-mounted spherical particles in open channel flow. *Phys. Fluids* **25**, 075103.

Cheng, N. & Law, A. W.-K. 2003 Fluctuations of turbulent bed shear stress. *J. Eng. Mech.* **129**, 126–130.

Ding, L. & Zhang, Q.-H. 2010 Lattice-Boltzmann simulation to characterize roughness effects of oscillatory boundary layer flow over a rough bed. *Coastal Engineering Proceedings,* pp. 1–11.

Einstein, H. 1950 *The bed-load function for sediment transportation in open channel flows.* Report, U.S. Dept. of Agriculture, Washington, DC.

Flores, N. & Sleath, J. 1998 Mobile layer in oscillatory sheet flow. *J. Geophys. Res.* **103** (C6), 12783.

Fornarelli, F. & Vittori, G. 2009 Oscillatory Boundary Layer Close to a Rough Wall. *Eur. J. Mech. B-Fluid* **28**, 283–295.

Fredsøe, J. & Deigaard, R. 1992 *Mechanics of Coastal Sediment Transport*. World Scientific.

Ghodke, C., Skitka, J. & Apte, S. 2014 Characterization of oscillatory boundary layer over a closely packed bed of sediment particles. *J. Comput. Mult. Flows* **6**, 447–456.

Hofland, B. & Battjes, J. 2006 Probability density function of instantaneous drag forces and shear stresses on a bed. *J. Hydraulic Eng.* **132**, 1169–1175.

Jensen, B., Sumer, B. & Fredsøe, J. 1989 Turbulent oscillatory boundary layers at high Reynolds numbers. *J. Fluid Mech.* **206**, 265–297.

Jeong, J. & Hussain, F. 2006 On the identification of a vortex. *J. Fluid Mech.* **285**, 69–94.

Keiller, D. & Sleath, J. 1976 Velocity measurements close to a rough plate oscillating in its own plane. *J. Fluid Mech.* **73**, 673–691.

Kim, J., Moin, P. & Moser, R. 2006 Turbulence statistics in fully developed channel flow at low Reynolds number. *J. Fluid Mech.* **177**, 133–166.

Nelson, J., Schmeeckle, M., Shreve, R. & McLean, S. 2000 Sediment entrainment

and transport in complex flows. *Selected Papers of the Int. Association for Hydraulic Research Symposium on River, Coastal and Estuarine Morphodynamics*.

Papanicolaou, A., Diplas, P., Evaggelopoulos, N. & Fotopoulos, S. 2002 Stochastic incipient motion criterion for spheres under various bed packing conditions. *J. Hydraulic Eng.* **128**, 369–380.

Sleath, J. 1995 Sediment transport by waves and currents. *J. Geophys. Res.* **100**, 10977.

Wu, F.-C. & Chou, Y.-J. 2003 Rolling and lifting probabilities for sediment entrainment. *J. Hydraulic Eng.* **129**, 110–119.

Wu, F.-C. & Kuo-Hsin, Y. 2004 Entrainment probabilities of mixed-size sediment incorporating near-bed coherent flow structures. *J. Hydraulic Eng.* **130**, 1187–1197.